UCRL-CONF-232584

LAWRENCE
LIVERMORE
NATIONAL
LABORATORY

Identifying Isotropic Events Using an Improved Regional Moment Tensor Inversion Technique

S. R. Ford, D. S. Dreger, W. R. Walter

July 9, 2007

Disclaimer

IDENTIFYING ISOTROPIC EVENTS USING AN IMPROVED REGIONAL MOMENT TENSOR INVERSION TECHNIQUE

Sean R. Ford[1], Douglas S. Dreger[1], William R. Walter[2]

University of California, Berkeley[1] and Lawrence Livermore National Laboratory[2]

ABSTRACT

Using a regional time-domain waveform inversion for the complete moment tensor we calculate the deviatoric and isotropic source components for several explosions at the Nevada Test Site as well as earthquakes, and collapses in the surrounding region of the western US. The events separate into specific populations according to their deviation from a pure double-couple and ratio of isotropic to deviatoric energy. The separation allows for anomalous event identification and discrimination between explosions, earthquakes, and collapses. Error in the moment tensor solutions and source parameters is also calculated.

We investigate the sensitivity of the moment tensor solutions to Green's functions calculated with imperfect Earth models, inaccurate event locations, and data with a low signal-to-noise ratio. We also test the performance of the method under a range of recording conditions from excellent azimuthal coverage to cases of sparse station availability, as might be expected for smaller events. Finally, we assess the depth and frequency dependence upon event size. This analysis will be used to determine the range where well-constrained solutions can be obtained.

OBJECTIVES

This research seeks to apply a regional distance complete moment tensor approach to tectonic, volcanic and man-made seismic events in order to document performance in the ability to identify and characterize anomalous (non-double-couple) seismic radiation. Identification of events with demonstrably significant non-double-couple components can aid in discrimination and possibly yield determination (Given and Mellman, 1986; Patton, 1988; Dreger and Woods, 2002). As an initial application we calculate the full moment tensors of 15 nuclear tests at the Nevada Test Site (NTS), three collapses (two mine collapses and one explosion cavity collapse), and 12 earthquakes near the NTS (Figure 1).

RESEARCH ACCOMPLISHED

We implement the time-domain full regional waveform inversion for the complete moment tensor (2nd rank tensor, M_{ij}) devised by Minson and Dreger (2007) after Herrmann and Hutcheson (1993) based on the work of Langston (1981). The complete moment tensor allows for a characterization of the relative amounts of deviatoric (M_{ij} where $i \neq j$) and isotropic (M_{ij} where $i=j$) source components, the similarity of those components with prior events in the source region, and a constraint on the source depth. The isotropic component is related to the volume change associated with a source (Muller, 1973), and in the case of an explosion this volume change is expected to be significant.

In general, synthetic seismograms are represented as the linear combination of fundamental Green's functions where the weights on these Green's functions are the individual moment tensor elements. The Green's functions for a one-dimensional (1-D) velocity model of eastern California and western Nevada (Song et al., 1996) are calculated as synthetic displacement seismograms using a frequency-wavenumber integration method (Saikia, 1994). The synthetic data is filtered with a 4-pole acausal Butterworth filter with a low-corner of 0.02 Hz and a high-corner of 0.05 Hz and 0.1 Hz for events with $M_W \geq 4$ and $M_W < 4$, respectively. At these frequencies, where the dominant wavelengths are approximately 100 km, we assume a point source for the low-magnitude regional events investigated in this study. The point source assumption allows for linearization in the time-domain, which is where we carry out the least-squares inversion. Data are collected for a total of 55 stations from the US National Seismic Network, IRIS/USGS, Berkeley Digital Seismic Network, Trinet, and the Lawrence Livermore National Laboratory (LLNL) network (Figure 1). We remove the instrument response, rotate to the great-circle frame, integrate to obtain displacement, and filter similarly to the synthetic seismograms.
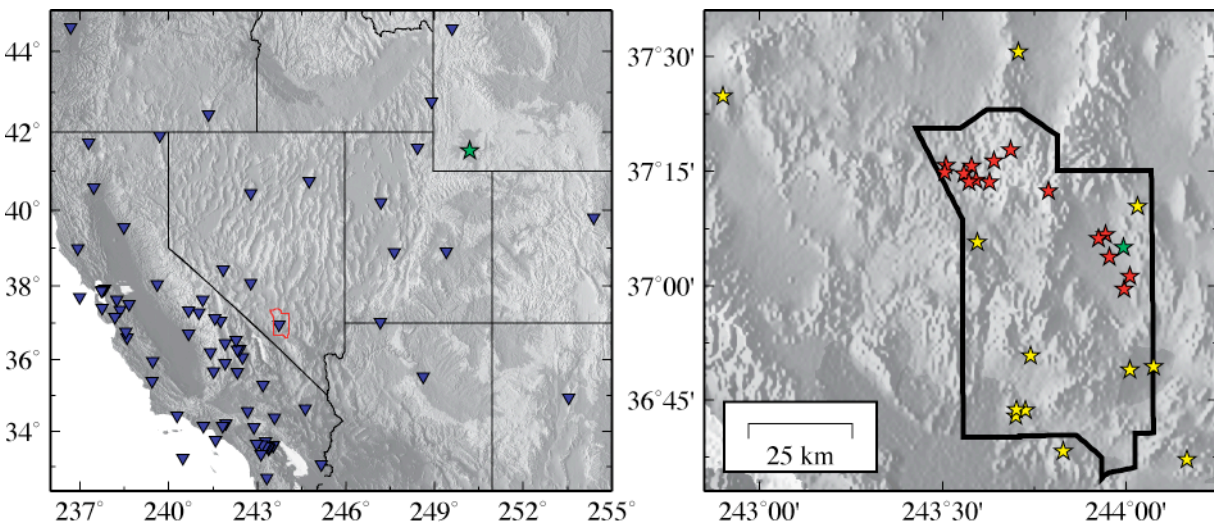

Figure 1. Maps of the Western US with stations (blue inverted triangles), earthquakes (yellow stars), explosions (red stars), and collapses (green stars) used in this study. The right panel shows a blow-up of the Nevada Test Site region, where the NTS is outlined in black. The NTS is also plotted in the left panel in red.

We calibrated the algorithm by calculating the full and deviatoric moment tensor for the 1992 Little Skull Mountain event. The deviatoric solution is obtained by constraining the trace of the moment tensor to be zero (M_{33} = -($M_{11}+M_{22}$)). Our result fits the data very well and is highly similar to the double-couple solution of Walter (1993), the deviatoric solution of Ichinose (2003), and the full solution of Dreger and Woods (2002). We calculate the full moment tensor of 12 earthquakes in the region near the Nevada Test Site (NTS, Figure 1). An example of the fit to the data for an aftershock of the 1992 Little Skull Mountain event is given in Figure 2a, where the moment tensor solution (Full) is decomposed to an isotropic (ISO) and deviatoric component ($M'_{ij} = M_{ij} - \delta_{ij} (M_{11}+M_{22}+M_{33})/3$). The deviatoric component is separated into a double-couple (DC) and compensated linear vector dipole (CLVD; Knopoff and Randall, 1970) that share the orientation of the major axis. The total scalar moment (M_0) is 2.23×10^{22} dyne-cm (M_W = 4.17). M_0 is equal to the sum of the isotropic moment ($M_{ISO} = (M_{11}+M_{22}+M_{33})/3$) and deviatoric moment (M_{DEV}), where all quantities are defined according to Bowers et al. (1999). The solution has a very small isotropic moment ($M_{ISO} = 1.39 \times 10^{21}$ dyne-cm) and there is little change between the Full and DC solutions. With the same algorithm we calculate the full moment tensors of 15 nuclear test explosions at the NTS (Figure 1). An example of the analysis is given by the solution for the 1991 HOYA test in Figure 2b. The largest component in the decomposition is isotropic and it contributes 59% of the total scalar moment.
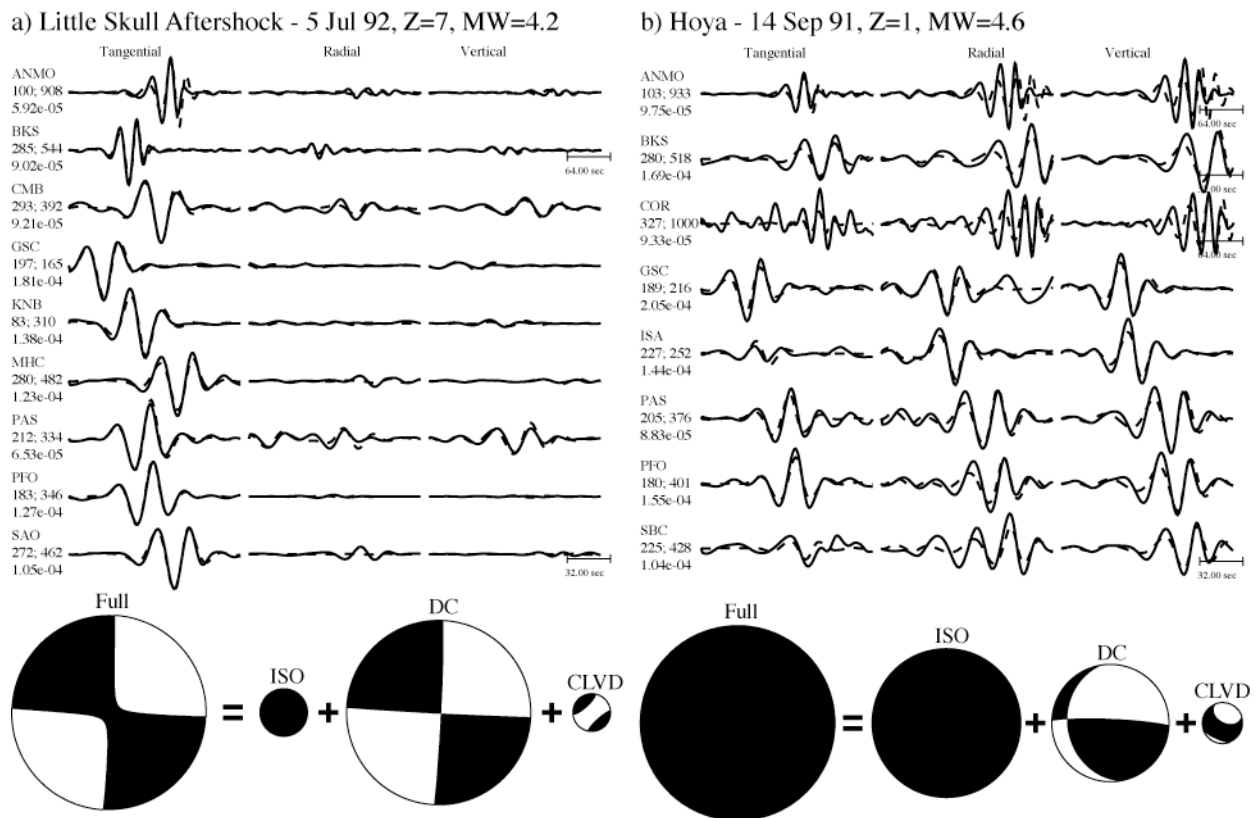
Figure 2. Moment tensor analysis of a) aftershock of the 1992 Little Skull Mt. event and b) the 1991 nuclear test, HOYA. The station name with azimuth; distance and maximum displacement (cm) are to the left of the data (solid line) and fit (dashed line) produced by inversion in the 20-50 s passband. Below the data is the full (Full) focal mechanism (lower hemisphere projection) which is decomposed to the isotropic (ISO) and deviatoric components, where the deviatoric component is separated into a double-couple (DC) and compensated linear vector dipole (CLVD) that share the orientation of the major axis. The area of the circles are relative to their scalar moment contribution. The largest component in the aftershock decomposition is the DC. The Full solution of the nuclear test is entirely compressive (black), which is due to the isotropic component contributing more than 50% of the total scalar moment.

a) Principal axes
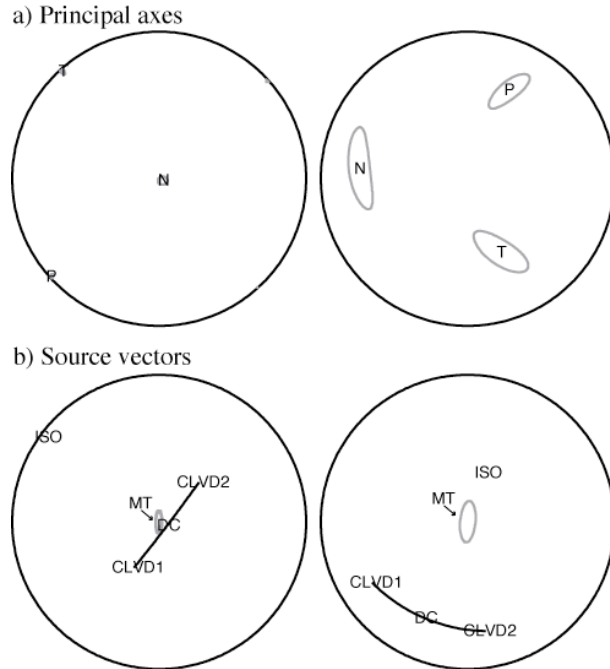
b) Source vectors

Figure 3. Principal axes analysis of the solutions for the Little Skull aftershock (left column) and NTS test HOYA (right column). a) Principal axes in the lower hemisphere projection and the associated 95% confidence region. b) Source vectors where the 95% confidence region of the MT vector is plotted in grey. The confidence region contacts the deviatoric subspace (defined as a line in the lower hemisphere projection between CLVD1 and CLVD2) for the earthquake solution but not for the explosion.

Mountain aftershock and NTS explosion, HOYA in Figure 3b. The general source vector, **MT**, for the Little Skull Mountain event lies very near the great-circle connecting the DC and CLVD vectors. This great-circle defines the subspace on which **MT** will lie if the source is purely deviatoric. The MT vector is also collinear with the DC vector, which is to say that the source is almost purely double-couple. The MT vector for the HOYA test lies well off the line defining the deviatoric solution space. The 95% confidence ellipse of **MT** is also plotted and it does not intersect the deviatoric solution space, which is to say that the solution has a significant isotropic component at the 95% confidence level. However, Riedesel and Jordan (1989) only consider perturbations to the principal moments and not the principal axes to construct confidence regions, which may be an inaccurate assumption if variance in the model parameters is great (Vasco, 1990). The proposed Monte Carlo approach described later is able to account for large variance.

Error in the moment tensor solutions is analyzed by plotting the best-fit and 95% confidence ellipses of the axes of minimum compression (**T**), maximum compression (**P**) and null (**N**), which are the eigenvectors of the symmetric moment tensor (Figure 3). The confidence ellipses are obtained from the model covariance matrix, where the variance is estimated by the residuals. In an effort to better characterize the source and confidence in the isotropic solution, we adopt the source vector convention described in Riedesel and Jordan (1989). Vectors are defined describing the general,

$$\mathbf{MT} = m_1\mathbf{T} + m_2\mathbf{N} + m_3\mathbf{P} \,,$$

double-couple,

$$\mathbf{DC} = \mathbf{T} - \mathbf{P} \,,$$

isotropic,

$$\mathbf{ISO} = \mathbf{T} + \mathbf{N} + \mathbf{P} \,,$$

and CLVD sources,

$$\mathbf{CLVD1} = \mathbf{T} - \mathbf{N}/2 - \mathbf{P}/2 \,;$$
$$\mathbf{CLVD2} = \mathbf{T}/2 + \mathbf{N}/2 - \mathbf{P} \,,$$

where m_1, m_2, and m_3 are the principal moments for the T, N, and P axes. Therefore, the source vectors are subspaces of the space defined by the eigenvectors of the moment tensor. The vectors are plotted on the focal sphere (similar to **T**, **N**, **P**) for the Little Skull
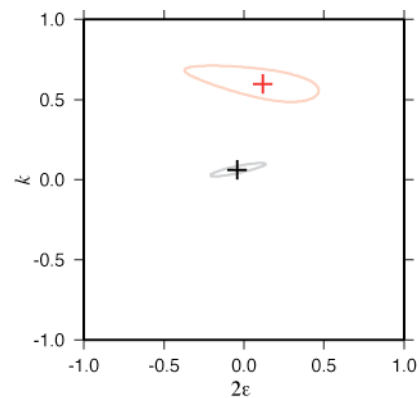
Figure 4. Source-type plot for the Skull Mt. aftershock (black) and NTS test HOYA (red) and the associated 95% confidence regions.

It is difficult to grasp the source-type from the standard focal mechanism plot. For example, one cannot discern the relative contributions of the isotropic and deviatoric components from the Full focal mechanism in Figure 2b. And decompositions of the deviatoric component are non-unique, where the DC and CLVD decomposition followed here could be replaced by two DCs (Julian et al., 1998). Following the source-type analysis described in Hudson et al. (1989) we calculate -2ε and k, which are given by

$$\varepsilon = \frac{-m_1'}{|m_3'|},$$

and

$$k = \frac{M_{ISO}}{|M_{ISO}| + |m_3'|},$$

where m_1', m_2' and m_3' are the deviatoric principal moments for the T, N, and P axes, respectively. ε is a measure of the departure of the deviatoric component from a pure double-couple mechanism, and is 0 for a pure double-couple and ± 0.5 for a pure CLVD. k is a measure of the volume change, where +1 would be a full explosion and -1 a full implosion. -2ε and k for the Little Skull Mountain aftershock and NTS explosion, HOYA are given in Figure 4,
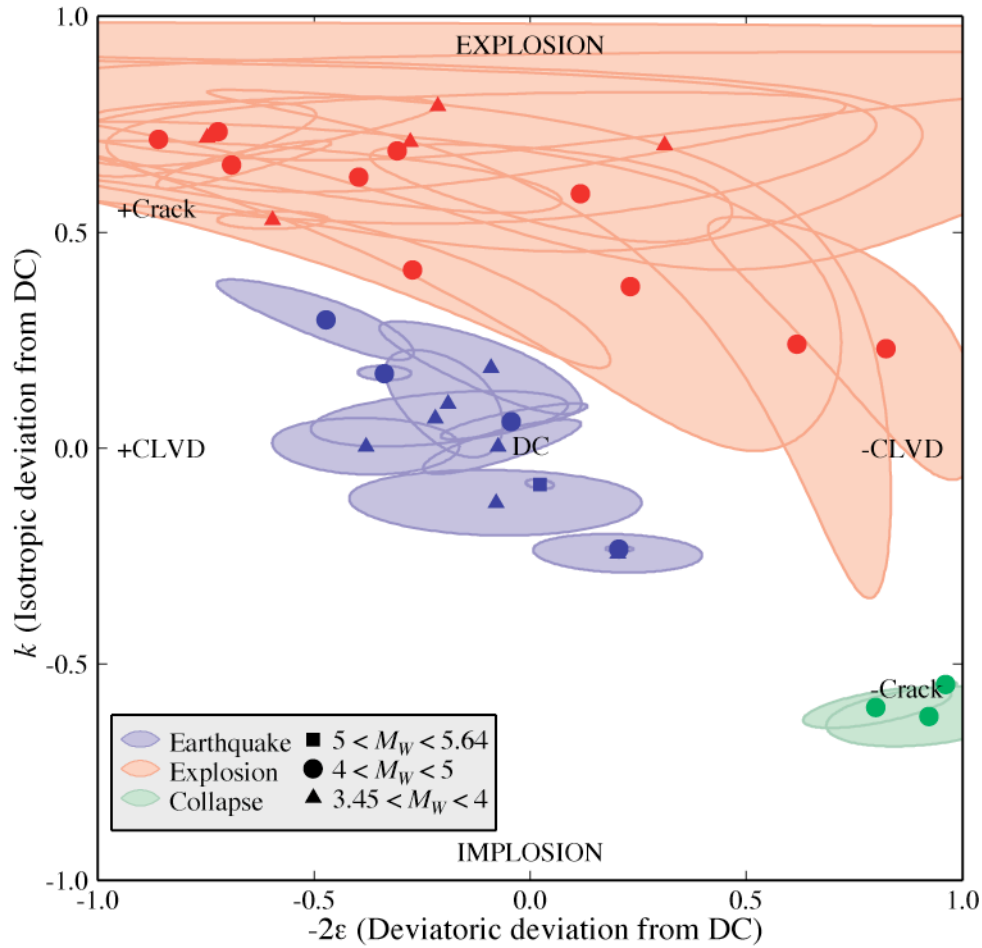
**Figure 5. Source-type plot of the 12 earthquakes (blue), 15 explosions (red), 3 collapses (green), and 14 events at the Long Valley Caldera (orange) and their associated 95% confidence regions (shaded) analyzed in this study. The magnitude of the event is given by the symbol. The abscissa measures the amount of volume change for the source and the ordinate measures the departure from a pure DC.**

where error in the values is derived as before. The earthquake is almost at the origin, which defines a pure DC, whereas the explosion is far from this point due to the large value of k.

We carry out similar analyses for three collapses (one cavity and two mine) and produce the source-type plot (Figure 5). The nuclear tests occupy the region where $k > 0.25$, the earthquakes cluster near the origin (with some interesting deviations), the collapses plot almost exactly at (1,-5/9), which is the location for a closing crack in a Poisson solid. The populations of earthquakes, explosions, and collapses separate in the source-type plot. These initial results are very encouraging and suggest a discriminant that employs the k, -2ε parameters. However, some of the 95% confidence regions for the explosions are very large and the solution is not well constrained. These events will be investigated further as described below. We also note that we limit explosions to those recorded by more than two stations at a broadband channel, thereby limiting the dataset to tests after Hornitos near the end of 1989. We hope to expand the dataset by making use of other digital data from the LLNL network.

The error analysis presented above is due to misfit of the data by the least-squares inversion. Part of the misfit may be due to nonstationary noise and we test the sensitivity of the inversion to increased noise with a series synthetic sources with varied signal-to-noise ratios (SNR). We find that a full explosion returns $k < 0.5$ only when SNR < 2 (Figure 6a). Typically, we use data with an SNR greater than 10. Another source of error not incorporated into the formal error analysis employed above is incorrectly calculated Green's functions due to ignorance of the true event depth and Earth structure. The analysis presented here attempts to find an optimal depth for the earthquakes by perturbing the reported depth a few kilometers, performing the inversion, and finding the best-fit solution. For all explosions and collapses the depth is fixed at 1 km. If this method were to be used for an event with an unknown source type, the depth could be an important source of error. We perform another synthetic test in which an explosion at 1 km is inverted with Green's functions calculated at varying depths. Surprisingly, we find that for an optimal station distribution $k > 0.5$ for depths up to 8 km (Figure 6b). Finally, we test how error in the Earth structure is mapped through the Green's functions to error in the solution. We use a simple 3-layer velocity model and vary the depth and velocities of those layers. We find that only for large variation in the layer velocity (>50%) can $k < 0.2$ be retrieved (Figure 6c). The solution is especially sensitive to the uppermost layer. Sileny et al. (2004) had a similar conclusion when investigating the deviatoric solution, where velocity perturbation of more than 30% and event depths mislocated by two times the actual depth return a well-resolved solution. Future work will identify what perturbations in the velocity model are the most significant given a station distribution and realistic noise considerations. A further consideration is the assumption of an isotropic Earth structure in the presence of anisotropic data, which may produce a spurious CLVD component (Sileny and Vavrycuk, 2002). Fortunately, the 1-D velocity model seems to be a good approximation in the presence of smoothly varying 3-D heterogeneity
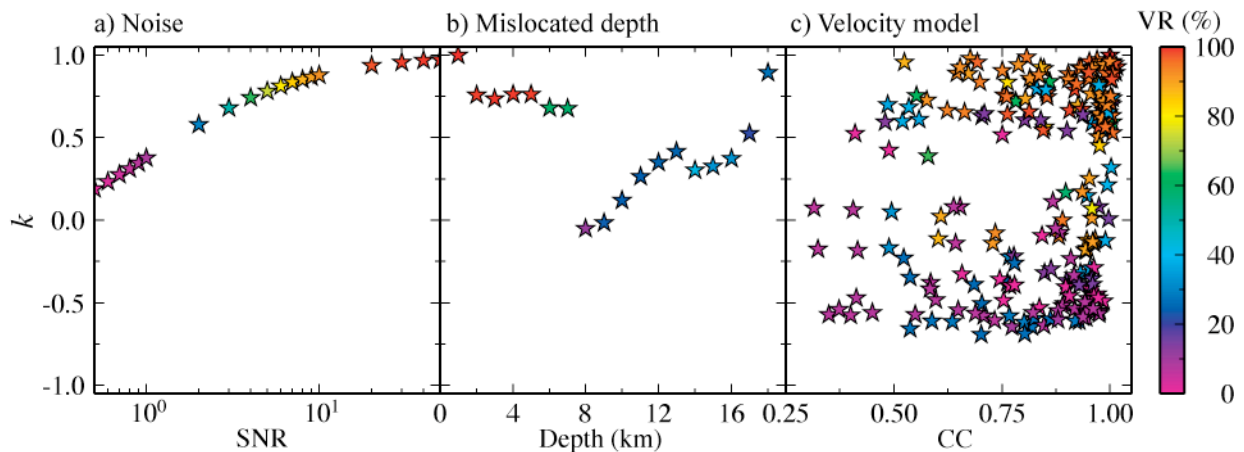
Figure 6. Sensitivity analysis for a synthetic explosion at a depth of 1 km in a three-layer 1D velocity model. a) Noise is added in the inversion. b) The inversion is carried out assuming an incorrect depth. c) The inversion is carried out for different three-layer velocity models where CC is the normalized correlation coefficient between the Green's functions for the correct velocity model and those of the incorrect velocity model used in the inversion. The symbols are colored as a function of variance reduction (VR).

(Panning et al., 2001).

Another consideration is the ability to resolve displacements for explosions near the surface. Since tractions normal to the vertical vanish at the free surface, the excitation coefficients associated with those tractions must vanish (Julian et al., 1998). Therefore at the free surface the moments of M_{13}, M_{23}, and the isotropic part of the M_{ij} cannot be resolved. Given and Mellman (1986) showed that at a source depth of 1 km the fundamental mode excitation functions associated with the moments listed previously effectively go to zero. We investigate the potential problems associated with traction vanishing at the free surface by inverting noisy data from a synthetic source composed of 60% explosion, 20% 45° dip-slip, and 20% vertical CLVD (as is commonly resolved for several NTS events) at a depth of 400 m in a three-layer 1D velocity model using Green's functions calculated at a depth of 1 km. Figure 6 shows that an explosive component can be resolved under favorable noise conditions, though with error in magnitudes of the moment tensor elements listed previously and M_{ISO} by almost 50%. At SNR < 10 considerable moment goes into M_{23} producing a significant vertical dip-slip component in the deviatoric source where there should be none. This provides a diagnostic for unresolved components in solutions, which can be seen in three of the most poorly resolved full moment tensors. This behavior is similar for events deeper than 300 m. At less than 200 m depth, the synthetic displacements become too small and the solution is unreliable.

CONCLUSIONS AND RECOMMENDATIONS

Nuclear test explosions from NTS and earthquakes from the surrounding region separate into specific populations according to source-type parameters, which are based on relative magnitudes of isotropic and deviatoric moments. The separation allows for anomalous event identification and discrimination between explosions, earthquakes, and collapses. Mislocation in depth on the order of a few kilometers and small deviations in a simple 1D velocity model still recovers a significant isotropic component, though Earth complexity is inadequately assessed by a three-layer structure. We also assess error due to vanishing traction at the free surface and are able to resolve a reliable solution at depths greater than 300 m, where error is expressed as an increasing vertical dip-slip component in the deviatoric solution.

A more complete treatment of the error introduced by ignorance of the event location and Earth structure can be given by a Monte Carlo approach, where several solutions are computed for a priori distributions of the hypocentral location and Earth model obtained from independent analyses. For example, confidence regions for a given hypocentral location as published by the NEIC can act as the a priori location distribution and the
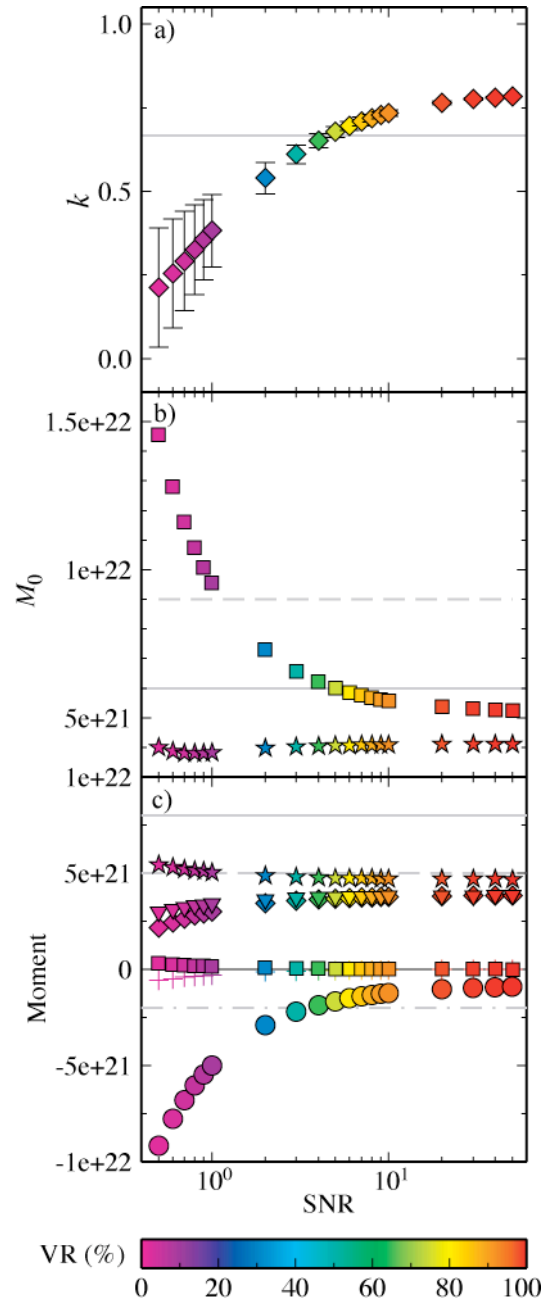
Figure 6. A noisy synthetic composite event at a depth of 400 m is inverted using Green's functions for an event at 1 km. a) Source-type parameter k, where the theoretical value is given by the grey line. b) M_0 (square) and M_{ISO} (star), where the theoretical values are given by the dashed and solid grey lines, respectively. c) M_{33} (star), M_{13} (cross), M_{23} (circle), M_{11} (diamond), M_{22} (triangle) and M_{12} (square) where theoretical values are given by the grey lines. Symbol color is the variance reduction (VR) of the solution.

hundreds of 1-D velocity models for a given region produced from a Markov Chain Monte Carlo method as in Pasyanos et al. (2006) can act as the velocity model distribution. Each of the moment tensor solutions could then be plotted producing a scatter density, which would aid in the understanding of how parameterization choice nonlinearly affects the moment tensor solutions, and help map the solution space of best-fit moment tensors. We will also search for solution dependence on individual measurements via Jackknife resampling of the data for specific stations and channels (Ichinose et al., 2003; Templeton and Dreger, 2006). Patton (1991) showed a correlation between yield and scalar moment for a given NTS region with events below the water table. Following this we hope to search for correlations based on the geophysical parameters given by Springer et al. (2002) for all NTS tests. We can also look at the principal axes of the explosions to see if they are responding to the regional stress environment, which may have important ramifications for understanding tectonic release coincident with nuclear tests. We will probe the tectonic contribution further in the context of the F-value, $F = \alpha^2/2\beta^2 \; M_{DEV}/M_{ISO}$, where α and β are the compressional and shear speeds of the medium, respectively. Toksoz and Kehrer (1972) showed that certain F-values can produce recordings of explosions with non-isotropic components similar to some observations. The explosions analyzed here do not have as much non-isotropic energy as has historically been observed at NTS and in other regions (Walter and Patton, 1990; Ekstrom and Richards, 1994). This may be due to the "wearing out" of the test site over time (Aki and Tsai, 1972), so we will expand the dataset of explosions to encompass other regions exhibiting exotic records like the "reversed" Rayleigh waves observed for the 1998 Indian tests (Walter et al., 1999).

ACKNOWLEDGEMENTS

REFERENCES

Aki, K. and Y.-B. Tsai (1972). Mechanism of love-wave excitation by explosive sources, J. Geophys. Res., 77(8), 1452-1475.

Bowers, D. and J.A. Hudson (1999). Defining the scalar moment of a seismic source with a general moment tensor, Bull. Seis. Soc. Amer., 89(5), 1390-1394.

Dreger, D. and B. Woods (2002). Regional distance seismic moment tensors of nuclear explosions; seismic source mechanism through moment tensors, Tectonophysics, 356(1-3), 139-156.

Dreger, D. S., H. Tkalcic, H., and M. Johnston (2000). Dilational processes accompanying earthquakes in the long valley caldera, Science, 288(5463), 122-125.

Ekstrom, G. and P.G. Richards (1994). Empirical measurements of tectonic moment release in nuclear-explosions from teleseismic surface-waves and body waves, Geophys. J. Int., 117(1), 120-140.

Given, J. W. and G.R. Mellman (1986). Estimating explosion and tectonic release source parameters of underground nuclear explosions from Rayleigh and Love wave observations, Tech. rep., Sierra Geophysics Report No. SGI-R-86-126, Kirkland, WA.

Herrmann, R. B. and K. Hutchensen (1993). Quantification of M_{Lg} for small explosion, Tech. rep., Phillips Laboratory Report PL-TR-93-2070.

Hudson, J. A., R. G. Pearce, R. G., and R. M. Rogers (1989). Source type plot for inversion of the moment tensor, J. Geophys. Res., 9(B1), 765-774.

Ichinose, G. A., J. G. Anderson, K. D. Smith and Y. Zeng (2003). Source parameters of Eastern California and Western Nevada earthquakes from regional moment tensor inversion, Bull. Seis. Soc. Amer., 93(1), 61-84.

Julian, B. R., A. D. Miller and G. R. Foulger (1998). Non-double-couple earthquakes; 1. Theory, Reviews of Geophysics, 36(4), 525- 549.

Knopoff, L. and M. J. Randall (1970). The compensated linear-vector dipole; a possible mechanism for deep earthquakes, J. Geophys. Res., 75(26), 4957-4963.

Langston, C. A. (1981). Source inversion of seismic waveforms; the Koyna, India, earthquakes of 13 September 1967, Bull. Seis. Soc. Amer., 71(1), 1-24.

Minson, S. and D. Dreger (2007). Improved seismic moment tensor inversion, Geophysics Jour- nal International.

Muller, G. (1973). Seismic moment and long-period radiation of underground nuclear explosions, Bull. Seis. Soc. Amer., 63(3), 847-857.

Panning, M., D. Dreger and H. Tkalcic (2001). Near-source velocity structure and isotropic moment tensors; a case study of the long valley caldera, Geophys. Res. Lett., 28(9), 1815-1818.

Pasyanos, M. E., G. A. Franz and A. L. Ramirez (2006). Reconciling a geophysical model to data using a Markov Chain Monte Carlo algorithm: An application to the Yellow Sea-Korean Peninsula region, J. Geophys. Res.-Solid Earth, 111(B3), B03313.

Patton, H. J. (1988). Source models of the Harzer explosion from regional observations of fundamental-mode and higher mode surface waves, Bull. Seis. Soc. Amer., 78(3), 1133-1157.

Patton, H. J. (1991). Seismic moment estimation and the scaling of the long-period explosion source spectrum, in Explosion Source Phenomenology, edited by S. R. Taylor.

Riedesel, M. and T. H. Jordan, T. H. (1989). Display and assessment of seismic moment tensors, Bull. Seis. Soc. Amer., 79(1), 85-100.

Saikia, C. K. (1994). Modified frequency-wavenumber algorithm for regional seismograms using Filon's quadrature; modelling of Lg waves in Eastern North America, Geophys. J. Int., 118(1), 142-158.

Sileny, J. (2004). Regional moment tensor uncertainty due to mismodeling of the crust, Tectonophysics, 383(3-4), 133-147.

Sileny, J. and V. Vavrycuk (2002). Can unbiased source be retrieved from anisotropic waveforms by using an isotropic model of the medium?; Seismic source mechanism through moment tensors, Tectonophysics, 356(1-3), 125-138.

Song, X. J., D. V. Helmberger and L. Zhao (1996). Broad-band modelling of regional seismograms; the basin and range crustal structure, Geophys. J. Int., 125(1), 15-29.

Springer, D. L., G. A. Pawloski, J. L. Ricca, R. F. Rohrer and D. K. Smith (2002). Seismic source summary for all U.S. below-surface nuclear explosions, Bull. Seis. Soc. Amer., 92(5), 1806-1840.

Templeton, D. C. and D. S. Dreger (2006). Non-double-couple earthquakes in the Long Valley volcanic region, Bull. Seis. Soc. Amer., 96(1), 69-79.

Toksoz, M. N. and H. H. Kehrer (1972). Tectonic strain release by underground nuclear explosions and its effect on seismic discrimination, Geophysical Journal of the Royal Astro- nomical Society, 31(1-3), 141-161.

Vasco, D. W. (1990). Moment-tensor invariants; searching for non-double-couple earthquakes, Bull. Seis. Soc. Amer., 80(2), 354-371.

Walter, W. R. (1993). Source parameters of the June 29, 1992 Little Skull Mountain earthquake from complete regional waveforms at a single station, Geophys. Res. Lett., 20(5), 403-406.

Walter, W. R. and H. J. Patton (1990). Tectonic release from the soviet joint verification experiment, Geophys. Res. Lett., 17(10), 1517-1520.

Walter, W. R., A. J. Rodgers, A. J and S. D. Malone (1999). Regional waveform modeling in Southwestern Asia; tectonic release from the May 11, 1998 Indian nuclear tests; SSA-99 94th annual meeting; Meeting abstracts, Seismological Research Letters, 70(2), 228.

Wessel, P., and W. H. F. Smith (1998). New, improved version of generic mapping tools released, in American Geophysical Union, San Francisco, Vol. 79, 579.